Film thickness versus misfit strain phase diagrams for epitaxial $PbTiO_3$ ultrathin ferroelectric films

Q. Y. Qiu and V. Nagarajan
School of Materials Science and Engineering, University of New South Wales, Sydney, New South Wales 2052, Australia

S. P. Alpay
Materials Science and Engineering Program and Institute of Materials Science, University of Connecticut, Storrs, Connecticut 06269, USA

(Received 1 June 2008; revised manuscript received 14 July 2008; published 27 August 2008)

We present a full scale nonlinear thermodynamic model based on a Landau-Ginzburg-Devonshire formalism and the theory of dense polydomain structures in a multiparameter space to predict the phase stability of (001) oriented $PbTiO_3$ epitaxial thin films as a function of film thickness and epitaxial strain. The developed methodology, which accounts for electrostatic boundary conditions as well as the formation of misfit dislocations and polydomain structures, produces a thickness-strain phase stability diagram where it finds that the rotational phases (the so-called *r* and *ac* phases) in epitaxial $PbTiO_3$ are possible only in a very small window. We find that for experimentally used thickness or strains (or both) that often fall outside this window, the film is in either single phase tetragonal (*c* phase) or in a *c*/*a*/*c*/*a* polydomain state; this explains why rotational polar domains are rarely observed in epitaxial ferroelectric thin films.

DOI: 10.1103/PhysRevB.78.064117 PACS number(s): 77.80.Bh, 77.84.Dy

I. INTRODUCTION

It is now universally accepted that mechanical and electrical boundary conditions control the ultimate phase stability in epitaxial ferroelectric thin films. Published papers show that compressive strains (in the plane of the film-substrate interface) may enhance the tetragonal out-of-plane polarization,[1,2] while tensile strains induce *in-plane* rotational phases of the polarization.[3] Recent breakthroughs that demonstrate substrate-based strain engineering as a powerful tool[4] include the recently reported strain induced ferroelectricity in $SrTiO_3$ (STO) (Refs. 5 and 6) and rotational phases in ultrathin $PbTiO_3$ (PTO),[3] both unique to the thin-film system and not generally found in the bulk parent compound under ambient conditions. It was also shown that the impact of in-plane compressive stresses is significantly more pronounced when the variations in the Curie transition temperature are compared with the polarization.[7] These observations are supported by theoretical studies that predict unconventional phases under large mechanical strains, in particular for in-plane tensile strains.[8–15] Concurrently, there has been significant progress in understanding the role of the electrical boundary conditions on the ultimate phase stability of ferroelectric thin films, including the role of the depolarization fields created due to the incomplete compensation of the polarization charges (even under the presence of real electrodes).[16–19] An interesting link between the mechanical as well as electrical boundary conditions is that the influence of both diminish with increasing thickness of the film, and not surprisingly thickness dependent evolution of ferroelectric phases (and related domain structures) forms an area of fascinating science as well as intense debate.[16,17,20–22]

Theoretical models reported so far treat these boundary and geometric (or size scaling) conditions as almost independent parameters. Treatments so far have ranged from first-principles methods focused on a fully commensurate interface with no provisions to include the possibility of ferroelastic domain or misfit dislocation formation to mean-field approaches for thick films with dense domains, which do not include the thickness dependence effects due to depolarization. For example, in the seminal work of Pertsev *et al.*,[23] which introduced the concept of the misfit strain phase diagrams based on the Landau-Ginzburg-Devonshire (LGD) mean-field theory (and further refined in Ref. 12), the authors explicitly include the role of strain[23] and later on the resultant ferroelastic domain evolution (referred to as the polydomain *c*/*a*/*c*/*a* type in this paper);[24] but the role of electrical boundary conditions and the thickness dependence of the strain was not discussed. Although *ab initio* methods did further modify the equilibrium phase stability diagrams in terms of the single domain phases[9,10] and even incorporated depolarization effects to the Pertsev diagram (demonstrated for $BaTiO_3$ ultrathin films[25]) as a function of thickness, these studies cannot account for the formation of misfit dislocations or ferroelastic polydomains, a key energy minimization process[26] that has been now universally observed in all thickness dependent experiments wherein the material undergoes a structural phase transformation. Indeed, phase field simulations that took into account both elastic and electrostatic boundary conditions, predicted phase stability that is markedly distinct from previous thermodynamic predictions.[27,28]

A commonality in all of the above is that the ferroelectric film is constrained by the underlying substrate and there are internal stresses due to epitaxy and the eigenstrain of the ferroelectric phase transformation. For the case of large internal stresses due to lattice misfit, this assumption can be inappropriate because these would be immediately relaxed by the generation of a periodic pattern of interfacial dislocations at the film-substrate interface at the growth temperature and by ferroelastic twin formation below the ferroelectric phase transformation temperature. Thus, the influence of the effective misfit strain must be applied with caution or its

effect may be heavily overestimated. For example, while phenomenological models as well as phase field models predict the rotational phases in PTO to be stable for a wide window of experimentally achievable in-plane tensile strains, these rotational variants for PTO have been observed only in a very special case of an ultrathin film (5 nm) on an orthorhombic substrate ($DyScO_3$),[3] and its formation might be related to the anisotropic in-plane strain state.[29–31] Furthermore, when the thickness of the ferroelectric was increased to greater than 10 nm, these rotational phases disappeared and the conventional $c/a/c/a$-type domain pattern was observed.[32]

In this paper, we present a full scale nonlinear thermodynamic model to analyze the phase stability of (001) oriented PTO epitaxial thin films that takes into account both thickness induced electrical boundary (depolarization field) effects as well as the real (effective misfit) strain in the films that incorporates the thickness dependent relaxation via the formation of misfit dislocation and ferroelastic polydomain patterns. We compute a universal free-energy functional and determine the most stable phase corresponding to the minimum minimorum for an epitaxial ferroelectric film that is sandwiched between electrodes in a *multiparameter* space (temperature, film thickness, effective misfit strain, critical thickness for dislocation formations, interface induced polarization gradients, and electrode screening length). Since the film is clamped between two symmetrical electrodes, we assume the polarization inside the film is centrally symmetrical along a z axis, along the film thickness resulting in zero gradient of polarization at the center. The mathematical approach is based on an Euler-Lagrangian framework detailed in our previous paper,[33] where we successfully predicted experimentally observed size scaling effects without the need for experimentally unmeasurable parameter of the extrapolation length. Indeed, the computed "film thickness-misfit strain" phase diagrams show that the rotational phases such as the *aa*, *ac*, or *r* phases appear in a very narrow range of misfit strain and thickness of the film. We find that for experimentally used thickness or strains (or both) that are often within this window, the film is a single phase tetragonal (c phase) or in a $c/a/c/a$ polydomain state.

II. THERMODYNAMIC ANALYSIS

We start our analysis with a generic renormalized Landau-Ginzburg-Devonshire free energy[30] of an epitaxial (001)-oriented monodomain ferroelectric thin film on a thick (001)-oriented cubic substrate;

$$\begin{aligned} G = {} & \frac{u_m^2}{s_{11}+s_{12}} + a_1^*(P_1^2+P_2^2) + a_3^* P_3^2 + a_{11}^*(P_1^4+P_2^4) + a_{33}^* P_3^4 \\ & + a_{12}^* P_1^2 P_2^2 + a_{13}^*(P_1^2+P_2^2)P_3^2 + a_{111}(P_1^6+P_2^6+P_3^6) \\ & + a_{112}[P_1^4(P_2^2+P_3^2) + P_2^4(P_1^2+P_3^2) + P_3^4(P_1^2+P_2^2)] \\ & + a_{123}(P_1P_2P_3)^2 + \frac{1}{2}g_{11}\left(\frac{dP_3}{dz}\right)^2 - \frac{1}{2}E_d P_3, \end{aligned} \tag{1}$$

where P_1 and P_2 are the in-plane polarizations (along x and y axes parallel to [100] and [010] directions of the substrate, respectively), P_3 is the out-of-plane polarization (i.e., along the [001] or the z axis), and a_i^*, a_{ij}^*, and a_{ijk} are the renormalized dielectric stiffness and higher-order dielectric coefficients,[23]

$$a_1 = \frac{T - T_0}{2\varepsilon_0 C}, \tag{2}$$

$$a_1^* = a_1 - u_m \frac{Q_{11}+Q_{12}}{s_{11}+s_{12}}, \tag{3}$$

$$a_3^* = a_1 - \frac{2Q_{12}u_m}{s_{11}+s_{12}}, \tag{4}$$

$$a_{11}^* = a_{11} + \frac{(Q_{11}^2+Q_{12}^2)s_{11} - 2Q_{11}Q_{12}s_{12}}{2(s_{11}^2 - s_{12}^2)}, \tag{5}$$

$$a_{12}^* = a_{12} - \frac{(Q_{11}^2+Q_{12}^2)s_{12} - 2Q_{11}Q_{12}s_{11}}{s_{11}^2 - s_{12}^2} + \frac{Q_{44}^2}{2s_{44}}, \tag{6}$$

$$a_{13}^* = a_{11} + \frac{Q_{12}(Q_{11}+Q_{12})}{s_{11}+s_{12}}, \tag{7}$$

$$a_{33}^* = a_{11} + \frac{Q_{12}^2}{s_{11}+s_{12}}, \tag{8}$$

where Q_{ij} are electrostrictive coefficients and s_{ij} are the elastic compliance coefficients at constant polarization. We also take into account in this analysis that the out-of-plane polarization is gradually terminated at the interface,[34] resulting in a polarization gradient in the case of incomplete charge screening. This necessitates the inclusion of a Ginzburg gradient coefficient g_{11} in the free-energy functional above. The lateral dimensions are much larger than the thickness and hence the gradients in the in-plane directions are neglected hereafter. We note that the free energy of the paraelectric phase has been taken arbitrarily as zero in the above relation; thus Eq. (1) can be thought of as an excess free energy due to polarization.

When computing the effect of thickness, the real misfit has to be used by taking into account relaxation via dislocations.[35,36] First, the pseudomorphic misfit strain, here on referred to as "numerical misfit strain," is calculated as $u_m^0 = (a_S - a_F)/a_S$ (where a_S and a_F are the substrate and film lattice parameters at the growth temperature T_G, respectively. The actual misfit strain (effective misfit) at this temperature as a function of thickness is given by

$$u_m(L) = 1 - \frac{(1-u_m^0)}{1 - u_m^0[1 - (L_c/L)]}, \tag{9}$$

where L is the film thickness and L_C is the Matthews-Blakeslee (MB) (Ref. 35) critical thickness for dislocation formation.[36]

The final term in Eq. (1) above is due to the depolarizing field given as

$$E_d = -\frac{\lambda(P_z - \langle P_3 \rangle)}{\varepsilon_0 \varepsilon_e (L/2)}, \tag{10}$$

where P_z is the polarization at the electrode interface ignoring the depolarizing field, $\langle P_3 \rangle$ is the average polarization along z axis, λ is the screening length of the electrode, ε_e is the dielectric constant of the electrode, and L is the film thickness.[33,37–40]

In order to determine the equilibrium polarization, we minimize Eq. (1) with respect to the polarization resulting in the Euler-Lagrange equation,

$$\frac{\partial G}{\partial P_i} - \frac{\partial}{\partial z}\frac{\partial G}{\partial\left(\frac{dP_i}{dz}\right)} = 0 \quad (i = 1,2,3), \tag{11}$$

with three solutions given by

$$\begin{aligned} &2a_1^* P_1 + 4a_{11}^* P_1^3 + 2a_{12}^* P_1 P_2^2 + 2a_{13}^* P_1 P_3^2 + 6a_{111} P_1^5 \\ &\quad + a_{112}[2P_1(P_2^4 + P_3^4) + 4P_1^3(P_2^2 + P_3^2)] \\ &\quad + 2a_{123} P_1 (P_2 P_3)^2 \\ &= 0, \end{aligned} \tag{12}$$

$$\begin{aligned} &2a_1^* P_2 + 4a_{11}^* P_2^3 + 2a_{12}^* P_2 P_1^2 + 2a_{13}^* P_2 P_3^2 + 6a_{111} P_2^5 \\ &\quad + a_{112}[2P_2(P_1^4 + P_3^4) + 4P_2^3(P_1^2 + P_3^2)] \\ &\quad + 2a_{123} P_2 (P_1 P_3)^2 \\ &= 0, \end{aligned} \tag{13}$$

$$\begin{aligned} g_{11}\frac{d^2 P_3}{dz^2} &= 2a_3^* P_3 + 4a_{33}^* P_3^3 + 2a_{13}^* P_3 (P_1^2 + P_2^2) + 6a_{111} P_3^5 \\ &\quad + a_{112}[2P_3(P_1^4 + P_2^4) + 4P_3^3(P_1^2 + P_2^2)] \\ &\quad + 2a_{123} P_3 (P_1 P_2)^2 - \frac{1}{2} E_d. \end{aligned} \tag{14}$$

The boundary condition $dP_i/dz|_{z=0}=0$ yields the polarization at the center, $P_i|_{z=0}=P_{0i}$. Furthermore, $d^2P_i/dz^2|_{z=0}$ can also be obtained from Eqs. (12)–(14). Only the perpendicular term of the polarization is expected to go to zero at the interface and thus we neglect dP_1/dz and dP_2/dz. Thus, after expansion of the polarization in terms of a Taylor series as shown below;

$$P_i(z) = P_i|_{z=0} + \left.\frac{dP_i}{dz}\right|_{z=0} z + \frac{1}{2!}\left.\frac{d^2P_i}{dz^2}\right|_{z=0} z^2 + \frac{1}{3!}\left.\frac{d^3P_i}{dz^3}\right|_{z=0} z^3 + \cdots. \tag{15}$$

We find that the in-plane polarizations inside the film scale as $P_1=P_{01}$ and $P_2=P_{02}$. The out-of-plane polarization is given as

$$\begin{aligned} P_3 &= P_{03} + \frac{z^2}{g_{11}}[a_3^* P_{03} + 2a_{33}^* P_{03}^3 + a_{13}^* P_{03}(P_{01}^2 + P_{02}^2) \\ &\quad + 3a_{111} P_{03}^5] + \frac{z^2 a_{112}}{g_{11}}[P_{03}(P_{01}^4 + P_{02}^4) + 2P_{03}^3(P_{01}^2 + P_{02}^2)] \\ &\quad + \frac{z^2 a_{123} P_{03}(P_{01}P_{02})^2}{g_{11}} - \frac{z^2 E_d}{4g_{11}}. \end{aligned} \tag{16}$$

To compute the polarizations P_{0i} at the center of the film, the depolarizing field can be neglected. However, it is critical to realize here that the polarization variation and the polarization at the center of the film are strongly dependent on the misfit strain and thus change with film thickness. This is because of the fact that the dielectric stiffness coefficients are altered due to the internal stresses. We note that in the presence of a nonzero epitaxial strain, the Curie temperature of the film T_C^{film} is given by a Clausius-Clapeyron-type relation,[41]

$$T_C^{\text{film}} = T_C^{\infty} + \frac{4u_m(L)\varepsilon_0 C Q_{12}}{s_{11} + s_{12}}, \tag{17}$$

where T_C^{∞} is the Curie temperature of the stress-free bulk ferroelectric.

If there is a relaxation of the epitaxial stresses via the formation of interfacial dislocations, the misfit strain experiences a decrease with increasing film thickness that can be simulated semiempirically via an exponential decay.[42–45] Recent experimental results[20,46] corroborate this as well and show that the transition temperature in ferroelectric films, even when the polarization is understood to have been fully stabilized due to screening by electrodes or polydomain formation, can be described via an empirical relationship[46] given as

$$T_C^{\text{film}} = \frac{T_C^{\infty}}{1 + \exp\left(-\sqrt{\frac{L}{\xi^*}}\right)}, \tag{18}$$

where ξ^* is the critical correlation length. We note here that this relation is for ultrathin PTO films on STO with negligible misfit and describes the thickness dependence of the transition temperature due to a polarization gradient that forms as a result of the finite screening length of the electrode when compared with bulk ferroelectric crystals. For ferroelectric films with larger misfits with respect to the underlying substrate, the thickness dependence of the misfit strain via the formation of misfit dislocations has to be taken into account as well. A self-consistent theoretical solution starting from a basic free-energy functional for a c-domain state that explicitly takes into account the stress relaxation and the screening effect of the electrode was developed recently[42] and its application to the present case is provided in the Appendix. The resultant analytical expression for T_C^{film} is given by

$$T_C^{\text{film}} = T_C^{\infty} - \sqrt[3]{\frac{27a_{33}^* \lambda^2 \varepsilon_0 C^3 (P_z - \langle P_3 \rangle)^2}{\varepsilon_e^2 L^2}} + \frac{4u_m(L)\varepsilon_0 C Q_{12}}{s_{11} + s_{12}}. \tag{19}$$

We are, therefore, in a position to compute the polarization at the center of the film. For this, we shall assume that the polarization gradient and the depolarizing field terms in Eq. (1) can be neglected. When the polarization is along one axis only, the equilibrium state is given by the equations of state corresponding to $\partial G/\partial P_i=0$, such that

$$a_i^* + 2a_{ii}^* P_i^2 + 3a_{111} P_i^4 = 0. \tag{20}$$

Therefore, the polarizations at the center of the film are

$$P_{0i} = \sqrt{\frac{-a_{ii}^* + \sqrt{a_{ii}^{*2} - 3a_{111}a_i^*}}{3a_{111}}}. \tag{21}$$

After obtaining the solutions of the polarization at the center of the film for monodomain phases, we can analyze the free energy for all possible phases and polydomain patterns as detailed below.

A. *c* phase ($P_1=P_2=0, P_3\neq 0$)

The free energy of the *c* phase is given by

$$G_c = \frac{u_m^2}{s_{11}+s_{12}} + a_3^* P_3^2 + a_{33}^* P_3^4 + a_{111} P_3^6 + \frac{1}{2} g_{11}\left(\frac{dP_3}{dz}\right)^2 - \frac{1}{2} E_d P_3. \tag{22}$$

In order to compare in dimensionless units, we rearrange the relative coordinate $\zeta=z/\xi^*$ to generate a universal function for all phases of the ferroelectric film. Let $p_3(\zeta)=P_3(z)/P_{S3}$ and $p_{03}=P_{03}/P_{S3}$ (where P_{S3} is the polarization of the thick film along the z axis) so that $dp_3/d\zeta=(\xi^*/P_{S3})(dP_3/dz)$ and $d^2p_3/d\zeta^2=(\xi^{*2}/P_{S3})(d^2P_3/dz^2)$.

Substitution of all values into Eq. (16) results to

$$p_{3c}(\zeta) = p_{03} + \left[\frac{a_3^*\xi^{*2}}{g_{11}} p_{03} + \frac{2a_{33}^*\xi^{*2}P_{S3}^2}{g_{11}} p_{03}^3 + \frac{3a_{111}\xi^{*2}P_{S3}^4}{g_{11}} p_{03}^5 + \frac{\lambda\xi^{*2}}{2\varepsilon_0\varepsilon_e L g_{11}}\left(\frac{P_z}{P_{S3}} - \frac{\langle P_3\rangle}{P_{S3}}\right)\right]\zeta^2. \tag{23}$$

The average polarization is then given by

$$\langle P_3\rangle = \frac{2}{L}\int_0^{L/2} P_3 dz. \tag{24}$$

The gradient term can be obtained by differentiating Eq. (23) and the energy of the depolarizing field follows from Eqs. (16) and (24); thus G_c can be determined.

B. *a* phase ($P_2=P_3=0, P_1\neq 0$)

The free energy of the single domain *a* phase is quite similar to the one of the *c* phase (but without the gradient terms), given as

$$G_a = \frac{u_m^2}{s_{11}+s_{12}} + a_1^* P_1^2 + a_{11}^* P_1^4 + a_{111} P_1^6. \tag{25}$$

Repeating the same procedure as for the *c* phase one can get $P_{1a}(\zeta)=P_{01}$. Similarly, for the orientational variant, the *a'* phase with $P_1=P_3=0$ and $P_2\neq 0$, we can replace P_1 with P_2 to get the appropriate solutions. Equation (25) yields the value for free energy of the *a* phase, G_a.

C. *aa* phase ($P_1=P_2\neq 0$ and $P_3=0$)

The *aa* phase is orthorhombic and the polarization vector is in the plane of the film-substrate interface with a polarization vector along the [110] direction. The depolarization field may be neglected; indeed phase field simulations show that the electrical and surface boundary conditions have little effect on the *aa* phase.[47] The free-energy density follows from

$$G_{aa} = \frac{u_m^2}{s_{11}+s_{12}} + a_1^*(P_1^2+P_2^2) + a_{11}^*(P_1^4+P_2^4) + a_{12}^* P_1^2 P_2^2 + a_{111}(P_1^6+P_2^6) + a_{112}(P_1^4P_2^2 + P_2^4P_1^2). \tag{26}$$

To solve the equation above analytically, we use two boundary conditions. First, the maximum value of the polarization is at the center of the ultrathin film and it will not take a value greater than the polarization of the thick film, i.e.,

$$\frac{P_{01}^2}{P_{S1}^2} + \frac{P_{02}^2}{P_{S2}^2} + \frac{P_{03}^2}{P_{S3}^2} = 1, \tag{27}$$

where P_{0i} are the center polarizations and P_{Si} are the polarizations of the thick film. Second, equilibrium is achieved when the gradients of the polarization are the same in all directions at the center of the film such that

$$\frac{\partial P_{\text{total}}}{\partial P_{01}} = \frac{\partial P_{\text{total}}}{\partial P_{02}} = \frac{\partial P_{\text{total}}}{\partial P_{03}}, \tag{28}$$

where $P_{\text{total}}=\sqrt{P_{01}^2+P_{02}^2+P_{03}^2}$.

Applying the first condition, we can solve the center polarization P_{01aa} and P_{02aa}. Hence, $P_{1aa}=P_{01aa}$ and $P_{2aa}=P_{02aa}$.

D. *ac* phase ($P_1\neq 0$, $P_3\neq 0$, and $P_2=0$)

Applying a similar formalism as in the case for the *aa* phase, we obtain the free energy as below;

$$G_{ac} = \frac{u_m^2}{s_{11}+s_{12}} + a_1^* P_1^2 + a_3^* P_3^2 + a_{11}^* P_1^4 + a_{33}^* P_3^4 + a_{13}^* P_1^2 P_3^2 + a_{111}(P_1^6+P_3^6) + a_{112}(P_1^4P_3^2 + P_3^4P_1^2) + \frac{1}{2} g_{11}\left(\frac{dP_3}{dz}\right)^2 - \frac{1}{2} E_d P_3. \tag{29}$$

With the help of Eqs. (27) and (28), we obtain the center polarizations of P_{01ac} and P_{03ac}. Hence, $P_{1ac}=P_{01ac}$. Substitution of all values into Eq. (16) results in

$$p_{3ac} = p_{03ac} + \frac{\xi^{*2}\zeta^2}{g_{11}P_{S3}}(a_3^* P_{03ac} + 2a_{33}^* P_{03ac}^3 + a_{13}^* P_{03ac}P_{01ac}^2 + 3a_{111}P_{03ac}^5) + \frac{\xi^{*2}\zeta^2}{g_{11}P_{S3}} a_{112}(P_{03ac}P_{01ac}^4 + 2P_{03ac}^3 P_{01ac}^2) + \frac{\lambda\xi^{*2}}{2\varepsilon_0\varepsilon_e L g_{11}}\left(\frac{P_z}{P_{S3}} - \frac{\langle P_{3ac}\rangle}{P_{S3}}\right)\zeta^2. \tag{30}$$

Similarly, for an $a'c$ phase with $P_2 \neq 0$, $P_3 \neq 0$, and $P_1 = 0$, we can replace P_1 with P_2 to get the appropriate solutions. We also define a $c'a'$ phase where the polarization of the c phase is inclined along a (110) plane such that the out-of-plane polarization at the center is equal in magnitude to the c phase and the in-plane polarization is equal to the a phase. Thus for the $c'a'$ phase we have $P_{03c'a'} = P_{03c}$ and $P_{01c'a'} = P_{01a}$.

E. r phase ($P_1 \neq 0, P_2 \neq 0, P_3 \neq 0$)

The r phase has essentially monoclinic symmetry and the free-energy functional contains all components of the polarization vector given by

$$\begin{aligned} G_r = {} & \frac{u_m^2}{s_{11}+s_{12}} + a_1^*(P_1^2+P_2^2) + a_3^* P_3^2 + a_{11}^*(P_1^4+P_2^4) + a_{33}^* P_3^4 \\ & + a_{12}^* P_1^2 P_2^2 + a_{13}^*(P_1^2+P_2^2)P_3^2 + a_{111}(P_1^6+P_2^6+P_3^6) \\ & + a_{112}[P_1^4(P_2^2+P_3^2) + P_2^4(P_1^2+P_3^2) + P_3^4(P_1^2+P_2^2)] \\ & + a_{123}(P_1P_2P_3)^2 + \frac{1}{2}g_{11}\left(\frac{dP_3}{dz}\right)^2 - \frac{1}{2}E_d P_3. \end{aligned} \tag{31}$$

Following a similar procedure yields the polarization vector at the center of the film with components P_{01r}, P_{02r}, and P_{03r}. Hence, $P_{1r} = P_{01r}$ and $P_{2r} = P_{02r}$. Substitution of all values into Eq. (16) results in

$$\begin{aligned} p_{3r} = {} & p_{03r} + \frac{\xi^{*2}\zeta^2}{g_{11}P_{S3}}[a_3^* P_{03r} + 2a_{33}^* P_{03r}^3 + a_{13}^* P_{03r}(P_{01r}^2 + P_{02r}^2) \\ & + 3a_{111}P_{03r}^5] + \frac{\xi^{*2}\zeta^2}{g_{11}P_{S3}} a_{112}[P_{03r}(P_{01r}^4 + P_{02r}^4) \\ & + 2P_{03r}^3(P_{01r}^2 + P_{02r}^2)] + \frac{\xi^{*2}\zeta^2}{g_{11}P_{S3}} a_{123}P_{03r}(P_{01r}P_{02r})^2 \\ & + \frac{\lambda\xi^{*2}}{2\varepsilon_0\varepsilon_e L g_{11}}\left(\frac{P_z}{P_{S3}} - \frac{\langle P_{3r}\rangle}{P_{S3}}\right)\zeta^2 \end{aligned} \tag{32}$$

The gradient term can be obtained by differentiating Eq. (32) and the depolarizing field follows from Eqs. (16) and (24).

F. Polydomain $a_1/a_2/a_1/a_2$ structure

The $a_1/a_2/a_1/a_2$ structure is a polydomain state that consists of a mixture of a_1 and a_2 domains with polarization components along the [100] and the [010] directions, respectively, resulting in an effective polarization parallel to the [110] in the film-substrate interface such that in average $P_1 \neq 0$, $P_2 \neq 0$, and $P_3 = 0$. Since the "microstresses" resulting from the indirect interaction across the twin interdomain interface act upon traction-free surfaces of the film, there is no additional energy associated with the formation of this polydomain state. As such, there is no critical thickness for the formation of this phase mixture and the polydomain structure consists of equal fractions of a_1 and the a_2 domains.[48] For an $a_1/a_2/a_1/a_2$ structure, since the domain fractions are equal, i.e., $\frac{1}{2}$, the total in-plane strain components are given by

$$u_1^T = u_2^T = u_m - \frac{1}{2}(Q_{11}P_1^2 + Q_{12}P_2^2). \tag{33}$$

Because a_1 and a_2 domains are orientational variants of the tetragonal ferroelectric phase, the polarization in each has to be equal to such that $P_{01} = P_{02} = P_S$. The overall polarization of the $a_1/a_2/a_1/a_2$ structure is then $\sqrt{2}P_S$. The excess elastic energy due to the formation of this polydomain pattern is

$$F_{\text{el}} = \frac{1}{S_{11}+S_{12}}\left[u_m - \frac{1}{2}P_S^2(Q_{11}+Q_{12})\right]^2. \tag{34}$$

The gradient term is neglected in the polarization expression as the film width and length are much larger than the film thickness and there are no electrodes on the sides of the film. The polarization of $a_1/a_2/a_1/a_2$ polydomains is hence the unsuppressed polarization at the center of the film, and thus $P_{0a1} = P_{01}$ and $P_{0a2} = P_{02}$. Hence, the Landau potential has the form;

$$G_{a1/a2} = a_1' P_S^2 + a_{11}' P_S^4 + a_{111}P_S^4 + \frac{u_m^2}{S_{11}+S_{12}}, \tag{35}$$

with

$$a_1' = a_1 - \frac{(Q_{11}+Q_{12})}{S_{11}+S_{12}}u_m, \tag{36}$$

and

$$a_{11}' = a_{11} + \frac{(Q_{11}+Q_{12})^2}{4(S_{11}+S_{12})}. \tag{37}$$

We note that the renormalized Landau coefficients above are identical to those derived by Koukhar and co-workers.[12,49]

G. Polydomain $c/a/c/a$ structure

As mentioned in the introduction, the rotational phases have been observed in very rare cases, while a $c/a/c/a$ polydomain structure made up of a mixture of c and a_1 or a_2 domains with polarization along the [001] and the [100] (or [010]) directions, respectively, is often observed experimentally if the effective misfit strain is tensile.[50,51] The formation of such a phase mixture has also been predicted theoretically in epitaxial ferroelectric films undergoing a cubic-tetragonal ferroelectric phase transformation.[21,36,52–55] There exists a critical film thickness for the formation of such a pattern due to the interplay between the internal stress relaxation and the microstresses that arise from the indirect interaction of the domains through the substrate.[55]

For a $c/a/c/a$ structure the equilibrium domain fraction in a ferroelectric film with a thickness much larger than the critical thickness of domain formation (h_C) when "translated" to our current notation is given by[55]

$$\phi_c^0 = 1 - \frac{(S_{11}-S_{12})(u_m - Q_{12}P_S^2)}{S_{11}(Q_{11}-Q_{12})P_S^2}. \tag{38}$$

The total free energy of the $c/a/c/a$ structure for a film with $L \gg h_C$ at the equilibrium domain fraction ϕ_c^0 ($0 < \phi_c^0 < 1$) is then simply

$$G_{c/a}(\phi_c^0) = a_1 P_S^2 + a_{11} P_S^4 + a_{111} P_S^6 + \frac{1}{2S_{11}}(u_m - Q_{12} P_S^2)^2$$

$$= \bar{a}_1 P_S^2 + \bar{a}_{11} P_S^4 + a_{111} P_S^6 + \frac{u_m^2}{2S_{11}}, \tag{39}$$

where

$$\bar{a}_1 = a_1 - \frac{Q_{12}}{S_{11}} u_m, \tag{40}$$

and

$$\bar{a}_{11} = a_{11} + \frac{Q_{12}^2}{2S_{11}}. \tag{41}$$

To take into account the thickness effect, one has to consider that the relaxation via the formation of this particular domain pattern does depend on the ratio of the film thickness to the critical thickness for domain formation, h_C/L. The thickness dependence of the equilibrium domain fraction and hence the degree of relaxation is given by[55]

$$\phi_c^0 = 1 - \frac{(S_{11} - S_{12})(u_m - Q_{12} P_S^2)}{S_{11}(1 - \sqrt{h_C/L})(Q_{11} - Q_{12}) P_S^2}, \quad 0 < \phi_c^0 < 1, \tag{42}$$

and the total free energy of the system is again given by $G_{c/a}(\phi_c^0)$ for $0 < \phi_c^0 < 1$. The polarization of each domain for a thick $c/a/c/a$ can then be computed as

$$P_{0S} = \sqrt{\frac{-\bar{a}_{11} + \sqrt{\bar{a}_{11}^2 - 3a_{111}\bar{a}_1}}{3a_{111}}}. \tag{43}$$

To consider the surface effect as well as the resultant depolarization field for the c domains of the $c/a/c/a$ polydomain mixture, we modify the potential as

$$G_{c/a}(\phi_c^0) = \bar{a}_1 P_S^2 + \bar{a}_{11} P_S^4 + a_{111} P_S^6 + \frac{u_m^2}{2S_{11}} + \phi_c^0 \left[\frac{1}{2} g_{11} \left(\frac{dP_S}{dz} \right)^2 - \frac{1}{2} E_d P_S \right]. \tag{44}$$

Again, this leads to

$$P_S(\zeta) = P_{0S} + \left[\frac{\bar{a}_1 \xi^{*2}}{\phi_c^0 g_{11}} P_{0S} + \frac{2\bar{a}_{11} \xi^{*2}}{\phi_c^0 g_{11}} P_{0S}^3 + \frac{3a_{111} \xi^{*2}}{\phi_c^0 g_{11}} P_{0S}^5 + \frac{\lambda \xi^{*2}}{2\varepsilon_0 \varepsilon_e L g_{11}} (P_z - \langle P_S \rangle) \right] \zeta^2. \tag{45}$$

We note here that other polydomain states could also be possible depending on to which ferroelectric phase the cubic paraelectric state transforms. The analysis in this and the previous sections assumes that a tetragonal ferroelectric phase forms below the critical temperature T_C^{film}. There are clearly more orientational variants of the orthorhombic and the rhombohedral phases, and should the material transform to one of these states, there are several other polydomain states that need to be considered. This is particularly important for example for $BaTiO_3$ films as $BaTiO_3$ in single-crystal form displays three ferroelectric phase transformations (cubic → tetragonal → orthorhombic → rhombohedral) with decreasing temperature. Internal stresses, therefore, might stabilize, for example, the orthorhombic phase over the tetragonal ferroelectric state. In such a case, more complicated twin structures may form.

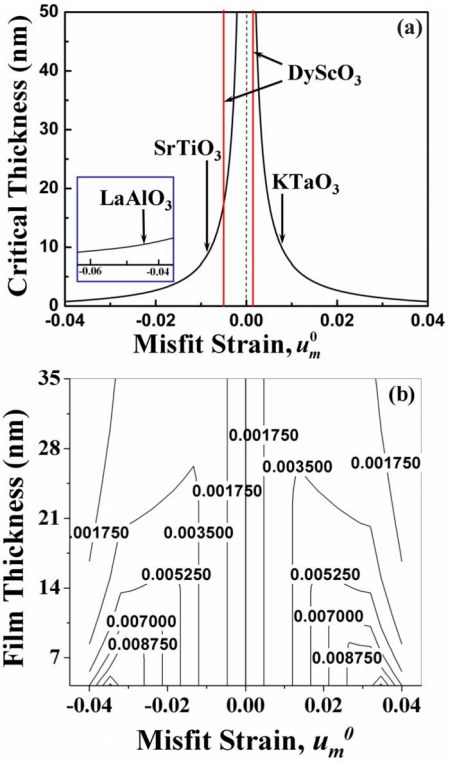

FIG. 1. (Color online) (a) Theoretical MB critical thickness for misfit dislocation formation in $PbTiO_3$ as a function of misfit strain at a growth temperature $T_G = 873$ K. The graph shows the respective MB critical thicknesses for popular substrates. (b) Computed contour map showing actual misfit strain as a function of thickness and the imposed numerical (pseudomorphic) misfit.

H. Paraelectric phase ($P_1 = P_2 = P_3 = 0$)

Finally, we also include the Landau potential for a paraelectric phase to account for the possibility that ferroelectric state would be unstable and that polarizations in no direction would be possible. This yields simply an elastic energy density given below;

$$G_p = \frac{u_m^2}{s_{11} + s_{12}}, \tag{46}$$

since the free energy of the unclamped stress-free paraelectric phase was taken arbitrarily as zero in the generalized LGD potential given in Eq. (1).

III. RESULTS AND DISCUSSION

Figure 1 plots the critical thickness for dislocation formation for epitaxial (001) PTO as a function of strain computed at the growth temperature T_G (873 K), with some of the more

popular oxide substrates that impose isotropic in-plane strains used so far in several experimental studies highlighted. We note that we use lattice parameters of both the film and the substrate at a growth temperature T_G=873 K. For the remainder of the paper, references to strains, unless specifically mentioned otherwise, correspond to the polarization-free effective in-plane strain, u_m. It is critical to start with this figure as it is vital to put into context the real effect of strain. Figure 1 displays the well understood exponential decay of the MB critical thickness for misfit dislocations as a function of the in-plane strain. Two key observations need to be highlighted for the purposes of the remainder of the paper: (i) the MB critical thickness is independent of the sign of the strain, i.e., both compressive and tensile strains have the same bearing, and (ii) it rapidly drops down to less than 5 nm for in-plane strains greater than 1% regardless whether the strain is compressive or tensile. Practically, this entails that for substrates such as STO (which imposes a 0.7% compressive strain in pseudomorphic films) and $KTaO_3$ (KTO, 0.9% tensile strain in pseudomorphic films), the effect of strain can be realized in the tens of nanometer thickness regime; on the other hand for $LaAlO_3$ or MgO substrates, which impose compressive strains of 4.5% or tensile strain of 7.2%, respectively, the critical thickness is so small (less than 1 nm) that for all practical purposes the in-plane strains would be relaxed partially via misfit dislocations even in ultrathin films. Figure 1(b) is a surface plot that illustrates the variation in the effective misfit, as a function of thickness and numerical strain. For purposes of symmetry, we plot only the magnitude of the effective misfit. In accordance with the MB concept, it shows that the misfit strain drops with increasing thickness and shows that practically, it is extremely rare to have more than 1% imposed strain for thin films under thermodynamic equilibrium.

Figure 2 plots the free energies for each of the phase (calculated at the center of the film) outlined in Sec. II above for four different film thickness, L, of PTO at room temperature (RT) (RT=298 K) as a function of misfit strain where, in fashion similar to the analysis presented in the first-principles work,[11] the modified free energies for each thickness are compared with trace of the fine details of each phase. The profiles are shown as a function of the numerical strain rather than the actual (real) strain because the actual strain varies with thickness and hence yields complex contours in the plot that would diminish the significance of the plot. However, while computing the profiles, values of the effective misfit strain as depicted in Fig. 1(b) were used. Numerical values of all fixed parameters and coefficients used in this analysis are provided in Table I. To avoid unnecessary complexities and elucidate the key findings here, we assume that the electrode (e.g., $SrRuO_3$ in this case) is pseudomorphic with the substrate. This assumption has little bearing on the criticality of the results discussed below and multiple relaxation mechanisms involving the electrode layer can be taken into account through a more complicated analysis[56] if the electrode were partially or completely relaxed.

Figures 2(a)–2(d) represent increasing film thickness from L=4, 8, 12, and 20 nm, respectively. It is found that these plots do not have the previously predicted smooth parabolic dependence on strain,[11] instead they have kinks at specific positions on the strain axis, which vary systematically as a function of thickness. The position of these kinks is indicated by vertical dashed lines, which moves closer to the origin with increasing thickness. Detailed inspection reveals that

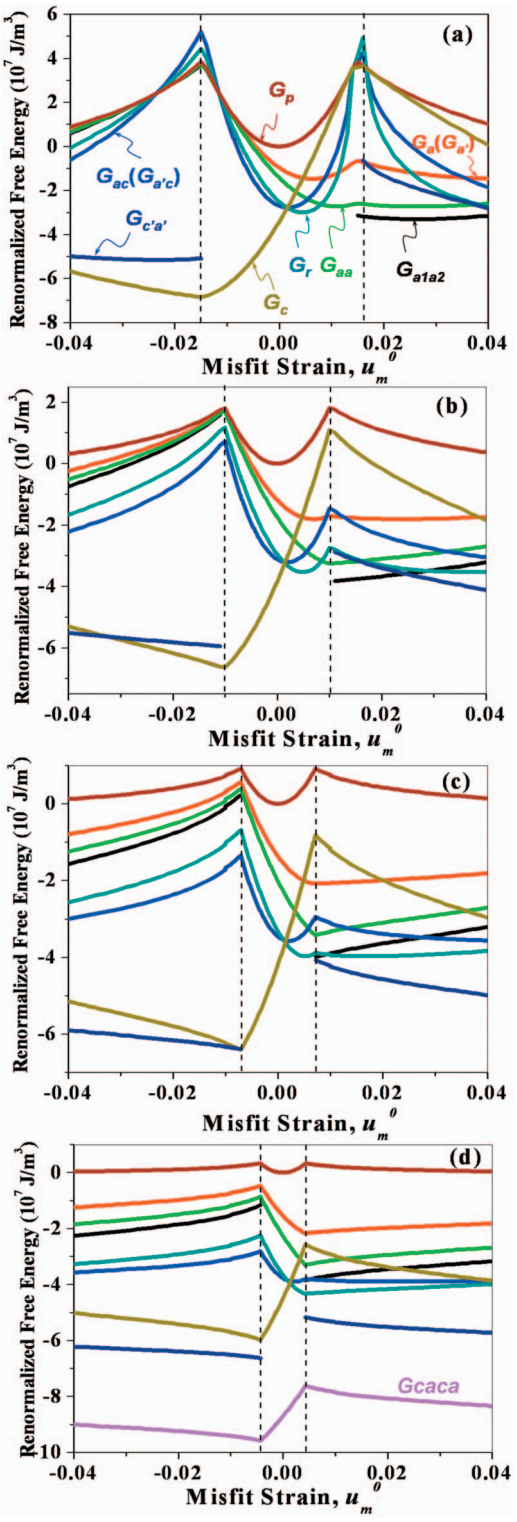

FIG. 2. (Color) Computed free-energy profiles as a function of misfit strain for each of the phases for different thickness; (a) L =4, (b) 8, (c) 12, and (d) 20 nm.

TABLE I. Thermodynamic, elastic, and electrostrictive coefficients for $PbTiO_3$; data compiled from Ref. 68.

a_1	$3.766(T-765.1)\times 10^5$(m/F)
a_{11}	-7.253×10^7(m^5/C^2 F)
a_{12}	7.50×10^8(m^5/C^2 F)
a_{111}	2.606×10^8(m^9/C^4 F)
a_{112}	6.10×10^8(m^9/C^4 F)
a_{123}	$-3.66E\times 10^9$(m^9/C^4 F)
Q_{11}	0.089(m^4/C^2)
Q_{12}	−0.026(m^4/C^2)
Q_{44}	0.0675(m^4/C^2)
s_{11}	8.00×10^{-12}(m^3 F/C^2)
s_{12}	-2.50×10^{-12}(m^3 F/C^2)
S_{44}	9.00×10^{-12}(m^3 F/C^2)
T_C^∞	765.1 (K)
C	1.50×10^5(°C)
ε_0	8.85×10^{-12}(C^2/N m^2)
ε_e	1
λ	2.3×10^{-11}(m)
a_F	3.96×10^{-10}(m)
ξ^*	1.4×10^{-9}(m)
g_{11}	3.35×10^{-9}(J m^3/C^2)
h_C	1.2×10^{-8}(m)

the position of the kinks in the plots actually corresponds to the limits for which the films are pseudomorphically constrained. Beyond these kinks the onset of dislocations reduces the elastic component of the free energy and thus induces a change in the sign of the energy profile. Within the vertical dashed lines where the imposed elastic strain is fully transferred to the film, one observes semblance to the parabolic profiles predicted in earlier papers.[11]

In Figs. 2(a)–2(c), the thickness is below the critical thickness for the polydomain $c/a/c/a$ formation. This thickness based on previous calculations[21,55,57] and experimental observations[51,58] is found to be 12–15 nm. For $L=4$ nm [Fig. 2(a)] the minimum point changes from a c phase to r phase, to aa phase, and finally to a $a_1/a_2/a_1/a_2$ polydomain state as one changes the misfit strain from compressive to tensile strains. In comparison, for slightly thicker film of $L=8$ nm [Fig. 2(b)] the minimum changes from the $c'a'$ rotational phase to c phase, to r phase, to $a_1/a_2/a_1/a_2$ polydomain state, and then back to a $c'a'$ phase with no aa phase. Figure 2(c) for $L=12$ nm demonstrates that the window for the monoclinic r phase is also now significantly narrowed and that the $a_1/a_2/a_1/a_2$ polydomain structure is no longer energetically favorable. Further significant changes are seen in Fig. 2(d) corresponding to $L=20$ nm, where the window for which the strains are pseudomorphically sustained by the film is very narrow and the influence of depolarization field is strongly diminished due to greater thickness. The formation of $c/a/c/a$ polydomain now seems unavoidable across the entire strain range. This can be understood as an effect of the elastic interaction of misfit dislocation with the ferroelastic domain walls and hence onset of ferroelastic domain nucleation from misfit dislocations, demonstrated both theoretically[59,60] as well as by transmission electron microscopy observations.[61–63] The phase profiles in Fig. 2 thus show that the rotational phases are more likely to be stable only for ultrathin films, which can sustain pseudomorphic strains as well as have a significant non-negligible component of the depolarizing field. These films also go through the attractive *rotational phase to polydomain state* transition, which could generate immensely large electromechanical strains as well as dielectric response.[24] For thicker films (e.g., those for which the film thickness is greater than 14 nm), polydomain $c/a/c/a$ is stable for the entire strain range. Interestingly the sole experimental finding that demonstrated the presence of rotational phases in PTO (Ref. 3) and $SrTiO_3$ (Ref. 6) is indeed for an ultrathin commensurately strained film.

Figure 3(a) is the computed film thickness-misfit strain phase diagram for the case of epitaxial PTO at room temperature; the (numerical) strain limits have been chosen with respect to the cubic oxide substrates that are commercially available. The limits of the thickness range are from a thickness of 4–35 nm. The lower limit is derived from the fact that below this thickness continuum mean-field approaches are no longer valid. For the upper limit, previous results show that epitaxial films of PTO greater than this thickness self-assemble into a cellular ferroelastic polydomain structure to minimize the internal elastic energy due to self-strain (i.e., tetragonality);[21,55,57] diminishing the primary role of substrate induced effects. The computed phase diagram employing the multiparameter model indicates phase stability that, although qualitatively similar, does have significant distinctions from previous results.[9,24] We focus first on films below the critical thickness for the formation of the $c/a/c/a$ polydomain. On the compressive side (negative misfit), as long as the film is below the critical thickness of polydomain formation and the MB critical thickness, the c phase is sustained. For films thicker than the MB thickness the onset of the rotational $c'a'$ phase is observed, which has not been predicted before. The $c'a'$ phase has been defined such that its out-of-plane and in-plane polarization components are equivalent to the c and a phases, respectively. Thus, structurally this phase can be attributed as an intermediate "finely mixed" phase, which sits at a phase transition between the fully c-axis oriented polarization state and the $c/a/c/a$ polydomain state. For ultrathin films below the MB regime under tensile misfits, the sequence of phase transformations follows $r\rightarrow aa\rightarrow a_1/a_2/a_1/a_2$, indicative of increasing inclination of the polarization vector toward the substrate-film interface with increasing tensile strain. The MB limit for both tensile and compressive misfits can be identified by the boundaries that determine the onset of the $c'a'$ phase.

Although the boundaries between the rotational phases are strongly dominated by the contours of the misfit strains Fig. 1(b), the sequence of phase transformations is dissimilar along the thickness and strain axes. In other words, going along equistrain contours along Fig. 1(b) does not yield the same phase in Fig. 3(a). This is because of the significant changes in the electrostatic boundary conditions as a function of increasing thickness. A critical point of consideration is that the model finds that the domain fractions (as well as

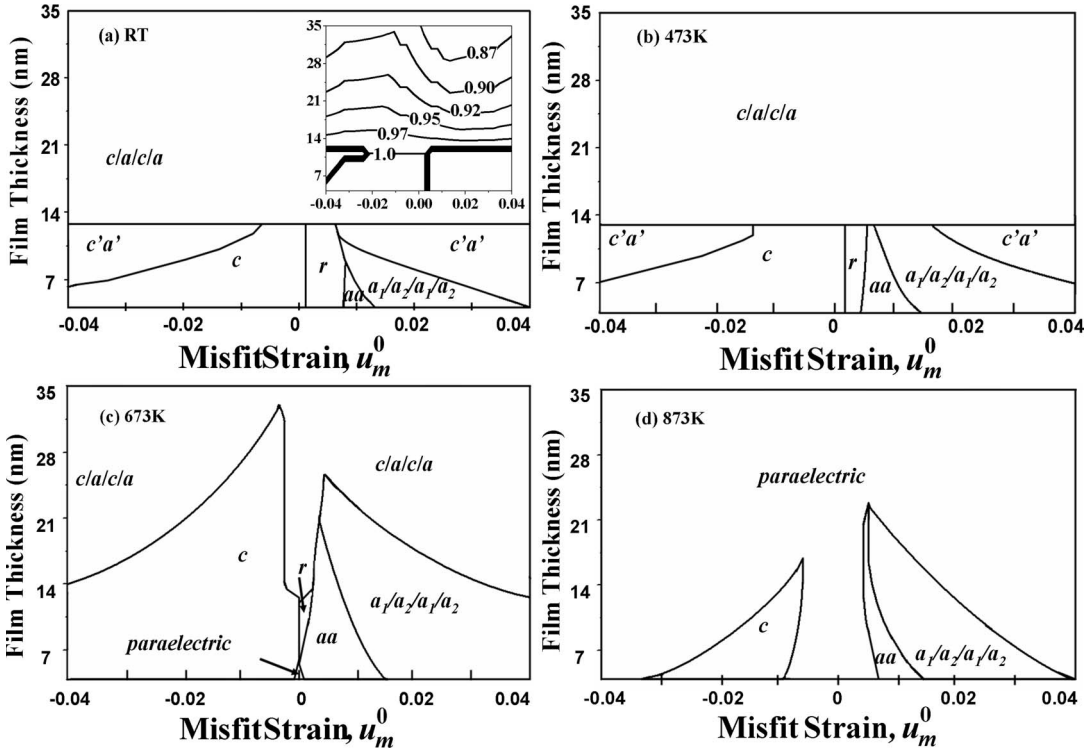

FIG. 3. (a) Film thickness-strain phase diagram for epitaxial [001] PTO as a function of numerical misfit strain. The y axis is the film thickness. The x axis is the numerical misfit strain calculated based on the paraelectric effective cubic lattice parameter of the ferroelectric and the substrate lattice parameter at growth temperature (T_G=873 K); the inset shows a contour map displaying the variation of the c-domain fraction ϕ_c^0 in the stability area of the $c/a/c/a$ polydomain pattern at RT in the same parameter space; (b) film thickness-strain phase diagram at 473, (c) 673, and (d) 873 K.

equilibrium polarization values) show a strong thickness as well as strain dependence. This is evident in the inset to Fig. 3(a), which is a three-dimensional surface plot of the calculated c-domain fraction (ϕ_c^0) as a function of film thickness as well as misfit strain at room temperature. We find that across the entire range where the polydomain state is stable, ϕ_c^0 decreases with increasing thickness and increasing tensile strain, in agreement with previous models.[21,55]

At higher temperatures [473, 673, and 873 K, Figs. 3(b)–3(d), respectively], the stability range for the rotational phases is significantly narrowed. The model finds that with increasing temperature [from Figs. 3(b)–3(d)] the $c'a'$ phase on the compressive side is systematically reduced and then eliminated; this is a consequence of the compressive misfit, which reduces the in-plane transition temperature T_1 that is defined as the critical temperature below which there is a ferroelectric instability associated with the appearance of in-plane polarization components P_1 and P_2. Hence, at temperatures greater than T_1 the film no longer carries in-plane polarization. With increased temperature, as an effect of the reduced polarization at higher temperatures, there is a concomitant decrease in the self-strain. This reduces the demand to decrease the excess elastic energy and hence even the range of polydomain $c/a/c/a$ is reduced. At the highest temperature (873 K, greater than the bulk ferroelectric transformation temperature of PTO), the only polar phase found stable on the compressive side is the c phase and its range of stability shows a marked resemblance to the strain relaxation plot in Fig. 1(a) and the strain contours in Fig. 1(b); (a) i.e., the c phase is found stable only in those areas where the actual misfit (and not the numerical misfit) is the highest. Thus it can be concluded that only in this range does a truly substrate induced compressive stress enhancement exist.

For films under tensile strains, we find that at 473 K the phase diagram is similar to the one at RT but with increased stability for the aa phase and decreased stability for the $c'a'$ phase as well as the r phase. This is an exact opposite of the compressive side; now the imposed tensile strain enhances T_1 and decreases the appearance of the out-of-plane polarization with a transition temperature T_3. This reduces and/or completely eliminates the stability of any phase with an out-of-plane polarization component, which is further clearly demonstrated at 673 K [Fig. 3(c)]. Here, the range for the r phase is drastically narrowed, and no other phase with an out-of-plane polarization component is found stable. Consequently, the stability range of aa phase and then the one of $a_1/a_2/a_1/a_2$ polydomain state increases. We also see beginnings of the paraelectric phase for ultrathin films around the origin where the transition temperature has been drastically reduced due to the depolarization field coupled with lack of mechanical strain to enhance polarization in either direction. At 873 K [Fig. 3(d)], the phase diagram illustrates beautifully the effect of externally imposed mechanical strain. Similar to the compressive side, only those thickness and temperature range where the effect of an in-plane tensile strain can be fully realized show a stable polar aa phase or

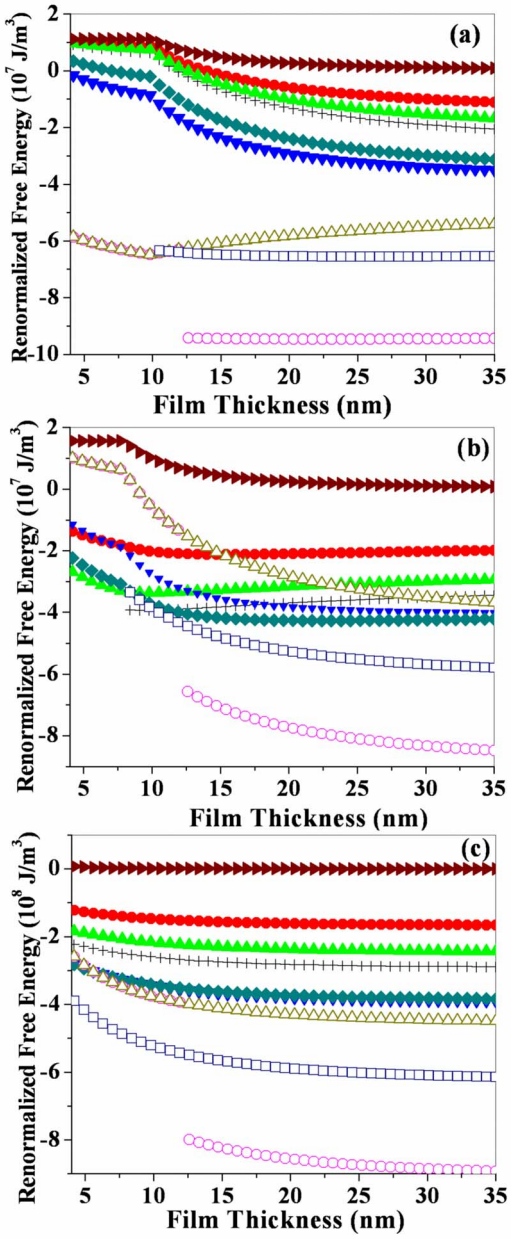

FIG. 4. (Color online) Computed free-energy profiles as a function of thickness for three different substrates. (a) STO, (b) KTO, and (c) MgO. Key to figure: G_{a1a2}—black +, $G_a(G_{a'})$—red ●, G_{aa}—green ▲, $G_{ac}(G_{a'c})$—blue ▼, G_r—dark cyan ◆, G_p—wine ▶, G_c—dark yellow Δ, G_{caca}—magenta ○, and $G_{c'a'}$—navy □.

$a_1/a_2/a_1/a_2$ polydomain mixture. We note that at these higher temperatures where the effect of depolarization field is negligible, the phase diagram looks very similar to the one obtained from thermodynamic calculations via the dense domain theory.[12]

Figures 4(a)–4(c) demonstrate the phase transition behavior for PTO deposited on three well investigated experimental substrates. Figure 4(a) is for a (001) STO substrate, which imposes −0.7% compressive misfit, Fig. 4(b) corresponds to (001) KTO substrate, which imposes a 0.9 % tensile misfit, and Fig. 4(c) is for a (001) MgO substrate, which imposes 7.2% tensile misfit in pseudomorphic PTO films. For the case of PTO on STO (at −0.7% compressive strain) we predict the c phase to be fully stable up to a thickness of 12 nm and then adapt a $c/a/c/a$ polydomain mixture, in agreement with previous thickness dependent predictions for PTO on STO.[50,51,58] For KTO, the sequence as a function of film thickness goes from aa phase, to $a_1/a_2/a_1/a_2$, to $c'a'$ phase, and then to a $c/a/c/a$ mixture. This can be linked to the tensile strain imposed by the substrate. Figure 4(c) for an MgO substrate shows first the $c'a'$ and then the $c/a/c/a$ polydomain structure as most stable; in complete agreement with experimental results and prior theoretical predictions.[50,51,58,64,65]

It is evident that the treatment for orthorhombic scandate substrates such as $GdScO_3$ or $DyScO_3$, which was the substrate used for the experimental observation of rotational polar domains in PTO,[3] has been omitted. For $DyScO_3$, experimental data shows that at growth temperature $DySO_3$ [110] imposes 0.1% and −0.4% strains along the two in-plane directions, respectively [see Fig. 1(a)], and hence the isotropic strain treatment presented herein is no longer applicable. Thus, one has to also consider the anisotropy (demonstrated experimentally)[29] and the kinetics of the misfit dislocation formation process, which would push both MB critical thicknesses as well as residual strain to larger values than the theoretical calculations. We also find that $c'a'$ phase (variant of the ac phase) is more stable than the r phase, which agrees with prior results.[3] Both rotational phases are found stable only for a thickness below 10–12 nm. Indeed, for a large tensile strains and the pertinent thickness of 5 nm, the model shows that rotational phases might be stabilized. Finally, one may also have to account for the stiffness of the underlying substrate. For example, Noheda and co-workers[32,66] show that $DyScO_3$ is clearly less stiff than STO and therefore the strain can be accommodated elastically better at the interface. The authors do report that for thicker films the rotational polar phase is lost and a polydomain structure is formed.[32] Our predictions are in agreement with this observation as well.

Recently rotational phases in bulk PTO were shown to be stabilized via the application of an external pressure.[67] However, in thin films, the phenomena of strain relaxation via dislocations and ferroelastic domains strongly controls and limits the formation of rotational phases. The importance of this effect is highlighted in Fig. 5, which plots the phase profiles for both tensile cases [Fig. 5(a) for KTO and Fig. 5(b) for MgO] when the strain is not allowed to relax via dislocations and hence it does not vary with thickness. Furthermore, the system was not allowed to relax by the formation of polydomain structures. Clearly the lowest (most stable) phase in this case is the in-plane orthorhombic aa phase under tensile misfits for both KTO and MgO, in agreement with previous theoretical predictions.[8,9,11,23,28] A secondary observation also is that in comparison to the phase profiles in Fig. 4, there are no "kinks" in profiles of Fig. 5 with free energies showing a smooth decay with increasing thickness.

IV. CONCLUSION

In summary, we presented a multiparameter Landau-Ginzburg-Devonshire formalism coupled with an elastic en-

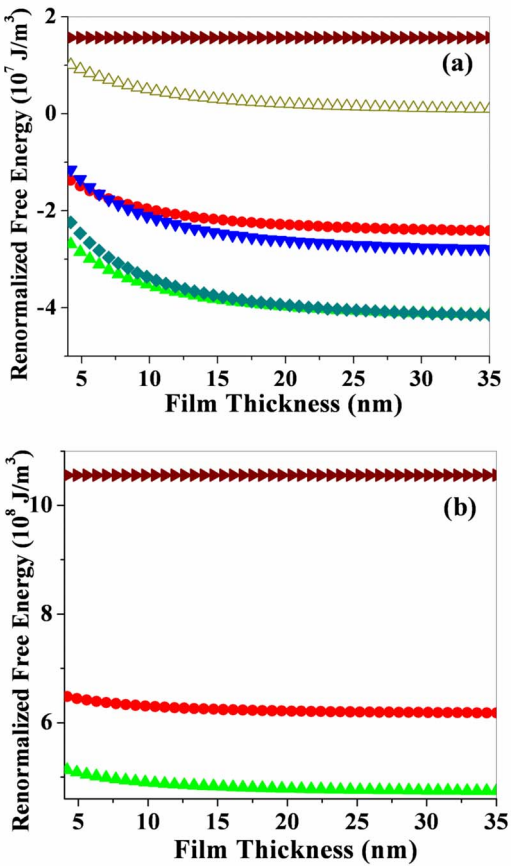

FIG. 5. (Color online) Phase profiles in PTO as a function of thickness for (a) KTO and (b) MgO. For these cases the film was forced to remain pseudomorphic and in a monodomain state. Due to these limitations, one now finds that only the *aa* phase to be the most stable. Symbols hold the same meaning as in Fig. 4.

ergy analysis via the dense domain theory and electrostatic considerations to show why rotational polar domains are very rare for the case of [001] epitaxial PTO thin films. Computed "thickness-strain" phase diagrams show that the rotational phases such as the *aa*, *ac*, or *r* phases may appear only in an extremely minute window of misfit strain and thickness of the film. We find that for experimentally employed thicknesses or strains (or both) that often fall outside this window, the film is either in the *c* phase or the $c/a/c/a$ or $a_1/a_2/a_1/a_2$ polydomain state.

ACKNOWLEDGMENTS

We would like to acknowledge the financial support from ARC Discovery through Grant No. DP 0666231 and Australian Academy of Science (V.N.). The work at UConn is supported by U.S. Army Research Office through Grant No. W911NF-05-1-0528. The authors acknowledge several stimulating conversations with B. Noheda and G. Catalan.

APPENDIX

We start off with the free energy of a *c*-domain structure as given below;

$$G_c = \frac{u_m^2}{s_{11}+s_{12}} + a_3^* P_3^2 + a_{33}^* P_3^4 + a_{111} P_3^6 + \frac{1}{2} g_{11}\left(\frac{dP_3}{dz}\right)^2 - \frac{1}{2} E_d P_3. \quad \text{(A1)}$$

The condition for thermodynamic equilibrium yields the following Euler-Lagrange equation:

$$g_{11}\frac{d^2P_3}{dz^2} = 2a_3^* P_3 + 4a_{33}^* P_3^3 + 6a_{111} P_3^5 - \frac{1}{2} E_d. \quad \text{(A2)}$$

We then integrate Eq. (A2) over z, such that

$$\frac{1}{2} g_{11}\left(\frac{dP_3}{dz}\right)^2 = a_3^*(P_3^2 - P_{03}^2) + a_{33}^*(P_3^4 - P_{03}^4) + a_{111}(P_3^6 - P_{03}^6) - \frac{1}{2} E_d (P_3 - P_{03}), \quad \text{(A3)}$$

with

$$E_d = -(P_z - \langle P_3 \rangle)\frac{\lambda}{\varepsilon_0 \varepsilon_e \frac{L}{2}}. \quad \text{(A4)}$$

Substitution of Eq. (A3) into Eq. (A1) results in

$$G_c = \frac{u_m^2}{s_{11}+s_{12}} + 2a_3^* P_3^2 + 2a_{33}^* P_3^4 + 2a_{111} P_3^6 - E_d P_3 - a_3^* P_{03}^2 - a_{33}^* P_{03}^4 - a_{111} P_{03}^6 + \frac{1}{2} E_d P_{03}. \quad \text{(A5)}$$

The thermodynamic equilibrium is given by $\partial G_c / \partial P_3 = 0$. Ignoring P^6 terms to obtain analytical expressions yields

$$4a_3^* P_3 + 8a_{33}^* P_3^3 = E_d. \quad \text{(A6)}$$

There are three solutions for the equation above as shown by Palova *et al.*[42] (also in chapter on Landau theory by Chandra and Littlewood in Ref. 69);

$$(P_3)_1 = \left(\frac{E_d}{2B} + \sqrt{R}\right)^{1/3} - \left(-\frac{E_d}{2B} + \sqrt{R}\right)^{1/3}, \quad \text{(A7)}$$

$$(P_3)_{2,3} = \frac{1}{2}(P_3)_1 \pm i\frac{\sqrt{3}}{3}\left[\left(\frac{E_d}{2B} + \sqrt{R}\right)^{1/3} + \left(-\frac{E_d}{2B} + \sqrt{R}\right)^{1/3}\right], \quad \text{(A8)}$$

where

$$R = \frac{A^3}{27B^3} + \frac{E_d^2}{4B^2}, \quad \text{(A9)}$$

with $A = 4a_3^*$ and $B = 8a_{33}^*$.

At the transition temperature R is equal to zero, such that

$$R = \frac{A^3}{27B^3} + \frac{E_d^2}{4B^2} = \frac{(4a_3^*)^3}{27(8a_{33}^*)^3} + \frac{4\lambda^2(P_z - \langle P_3 \rangle)^2}{\varepsilon_0^2 \varepsilon_e^2 L^2 4(8a_{33}^*)^2} = 0, \quad \text{(A10)}$$

and thus

$$a_3^* = -\sqrt[3]{\frac{27\lambda^2 a_{33}^*(P_z - \langle P_3\rangle)^2}{8\varepsilon_0^2\varepsilon_e^2 L^2}}. \tag{A11}$$

The renormalized dielectric stiffness a_3^* is

$$a_3^* = a_1 - \frac{2u_m Q_{12}}{s_{11}+s_{12}}, \tag{A12}$$

and a_1 obeys the Curie-Weiss law;

$$a_1 = \frac{T - T_c^\infty}{2\varepsilon_0 C}, \tag{A13}$$

where C is the Curie-Weiss constant, ε_0 is the permittivity of vacuum, T is the temperature, and T_C^∞ is the Curie temperature of the stress-free bulk ferroelectric. Substitution of Eqs. (A12) and (A13) into Eq. (A11) at $T=T_C^{\text{film}}$ yields

$$\frac{T_C^{\text{film}} - T_C^\infty}{2\varepsilon_0 C} - \frac{2u_m Q_{12}}{s_{11}+s_{12}} = -\sqrt[3]{\frac{27a_{33}^*\lambda^2(P_z - \langle P_3\rangle)^2}{8\varepsilon_0^2\varepsilon_e^2 L^2}}. \tag{A14}$$

The transition temperature of the film is then given by

$$T_C^{\text{film}} = T_C^\infty - \sqrt[3]{\frac{27a_{33}^*\lambda^2\varepsilon_0 C^3(P_z - \langle P_3\rangle)^2}{\varepsilon_e^2 L^2}} + \frac{4u_m(L)\varepsilon_0 C Q_{12}}{s_{11}+s_{12}}. \tag{A15}$$

[1] A. L. Roytburd, S. P. Alpay, V. Nagarajan, C. S. Ganpule, S. Aggarwal, E. D. Williams, and R. Ramesh, Phys. Rev. Lett. **85**, 190 (2000).
[2] C. Ederer and N. A. Spaldin, Phys. Rev. Lett. **95**, 257601 (2005).
[3] G. Catalan, A. Janssens, G. Rispens, S. Csiszar, O. Seeck, G. Rijnders, D. H. A. Blank, and B. Noheda, Phys. Rev. Lett. **96**, 127602 (2006).
[4] D. G. Schlom, L. Q. Chen, C. B. Eom, K. M. Rabe, S. K. Streiffer, and J. M. Triscone, Annu. Rev. Mater. Res. **37**, 589 (2007).
[5] J. H. Haeni, P. Irvin, W. Chang, R. Uecker, P. Reiche, Y. L. Li, S. Choudhury, W. Tian, M. E. Hawley, B. Craigo, A. K. Tagantsev, X. Q. Pan, S. K. Streiffer, L. Q. Chen, S. W. Kirchoefer, J. Levy, and D. G. Schlom, Nature (London) **430**, 758 (2004).
[6] A. Vasudevarao, S. Denev, M. D. Biegalski, Y. Li, L.-Q. Chen, S. Trolier-McKinstry, D. G. Schlom, and V. Gopalan, Appl. Phys. Lett. **92**, 192902 (2008).
[7] H. N. Lee, S. M. Nakhmanson, M. F. Chisholm, H. M. Christen, K. M. Rabe, and D. Vanderbilt, Phys. Rev. Lett. **98**, 217602 (2007).
[8] N. A. Pertsev, V. G. Kukhar, H. Kohlstedt, and R. Waser, Phys. Rev. B **67**, 054107 (2003).
[9] C. Bungaro and K. M. Rabe, Phys. Rev. B **69**, 184101 (2004).
[10] O. Diéguez, S. Tinte, A. Antons, C. Bungaro, J. B. Neaton, K. M. Rabe, and D. Vanderbilt, Phys. Rev. B **69**, 212101 (2004).
[11] O. Dieguez, K. M. Rabe, and D. Vanderbilt, Phys. Rev. B **72**, 144101 (2005).
[12] V. G. Kukhar, N. A. Pertsev, H. Kohlstedt, and R. Waser, Phys. Rev. B **73**, 214103 (2006).
[13] I. B. Misirlioglu, S. P. Alpay, F. He, and B. O. Wells, J. Appl. Phys. **99**, 104103 (2006).
[14] Y. L. Li, S. Choudhury, J. H. Haeni, M. D. Biegalski, A. Vasudevarao, A. Sharan, H. Z. Ma, J. Levy, V. Gopalan, S. Trolier-McKinstry, D. G. Schlom, Q. X. Jia, and L. Q. Chen, Phys. Rev. B **73**, 184112 (2006).
[15] Y. L. Li and L. Q. Chen, Appl. Phys. Lett. **88**, 072905 (2006).
[16] J. Junquera and P. Ghosez, Nature (London) **422**, 506 (2003).
[17] C. Lichtensteiger, J.-M. Triscone, J. Junquera, and P. Ghosez, Phys. Rev. Lett. **94**, 047603 (2005).
[18] I. Kornev, H. Fu, and L. Bellaiche, Phys. Rev. Lett. **93**, 196104 (2004).
[19] C. G. Duan, R. F. Sabirianov, W. N. Mei, S. S. Jaswal, and E. Y. Tsymbal, Nano Lett. **6**, 483 (2006).
[20] D. D. Fong, G. B. Stephenson, S. K. Streiffer, J. A. Eastman, O. Auciello, P. H. Fuoss, and C. Thompson, Science **304**, 1650 (2004).
[21] W. Pompe, X. Gong, Z. Suo, and J. S. Speck, J. Appl. Phys. **74**, 6012 (1993).
[22] V. Nagarajan, J. Junquera, S. Prasertchoung, J. Q. He, C.-L. Jia, K. L. Y. K. Kim, M. Dawber, T. Zhao, H. Kohlstedt, P. Ghosez, K. M. Rabe, S. Baik, R. Ramesh, and R. Waser, J. Appl. Phys. **100**, 051609 (2006).
[23] N. A. Pertsev, A. G. Zembilgotov, and A. K. Tagantsev, Phys. Rev. Lett. **80**, 1988 (1998).
[24] N. A. Pertsev and V. G. Koukhar, Phys. Rev. Lett. **84**, 3722 (2000).
[25] Bo-Kuai Lai, I. A. Kornev, L. Bellaiche, and G. J. Salamo, Appl. Phys. Lett. **86**, 132904 (2005).
[26] A. L. Roitburd, Phys. Status Solidi A **37**, 329 (1976).
[27] Y. L. Li, S. Y. Hu, Z. K. Liu, and L. Q. Chen, Appl. Phys. Lett. **81**, 427 (2002).
[28] Y. L. Li, S. Choudhury, Z. K. Liu, and L. Q. Chen, Appl. Phys. Lett. **83**, 1608 (2003).
[29] W. K. Simon, E. K. Akdogan, and A. Safari, J. Appl. Phys. **97**, 103530 (2005).
[30] A. G. Zembilgotov, N. A. Pertsev, U. Bottger, and R. Waser, Appl. Phys. Lett. **86**, 052903 (2005).
[31] I. B. Misirlioglu, G. Akcay, S. Zhong, and S. P. Alpay, J. Appl. Phys. **101**, 036107 (2007).
[32] S. Venkatesan, B. J. Kooi, J. T. M. De Hosson, A. H. G. Vlooswijk, and B. Noheda, J. Appl. Phys. **102**, 104105 (2007).
[33] Q. Y. Qiu and V. Nagarajan, J. Appl. Phys. **102**, 104113 (2007).
[34] R. Kretschmer and K. Binder, Phys. Rev. B **20**, 1065 (1979).
[35] J. W. Matthews and A. E. Blakeslee, J. Cryst. Growth **27**, 118 (1974).
[36] J. S. Speck and W. Pompe, J. Appl. Phys. **76**, 466 (1994).
[37] R. R. Mehta, B. D. Silverman, and J. T. Jacobs, J. Appl. Phys.

44, 3379 (1973).
[38] A. M. Bratkovsky and A. P. Levanyuk, Phys. Rev. B **63**, 132103 (2001).
[39] M. D. Glinchuk, E. A. Eliseev, V. A. Stephanovich, and R. Farhi, J. Appl. Phys. **93**, 1150 (2003).
[40] A. M. Bratkovsky and A. P. Levanyuk, Appl. Phys. Lett. **89**, 253108 (2006).
[41] A. G. Zembilgotov, N. A. Pertsev, H. Kohlstedt, and R. Waser, J. Appl. Phys. **91**, 2247 (2002).
[42] L. Palova, P. Chandra, and K. M. Rabe, Phys. Rev. B **76**, 014112 (2007).
[43] H. J. Kim, S. H. Oh, and H. M. Jang, Appl. Phys. Lett. **75**, 3195 (1999).
[44] L. J. Sinnamon, M. M. Saad, R. M. Bowman, and J. M. Gregg, Appl. Phys. Lett. **81**, 703 (2002).
[45] G. Catalan, B. Noheda, J. McAneney, L. J. Sinnamon, and J. M. Gregg, Phys. Rev. B **72**, 020102(R) (2005).
[46] D. D. Fong, A. M. Kolpak, J. A. Eastman, S. K. Streiffer, P. H. Fuoss, G. B. Stephenson, C. Thompson, D. M. Kim, K. J. Choi, C. B. Eom, I. Grinberg, and A. M. Rappe, Phys. Rev. Lett. **96**, 127601 (2006).
[47] Y. L. Li, S. Y. Hu, and L. Q. Chen, J. Appl. Phys. **97**, 034112 (2005).
[48] A. L. Roytburd, in *Thin Film Ferroelectric Materials and Devices*, edited by R. Ramesh (Kluwer, Norvell, MA, 1997), p. 71.
[49] V. G. Koukhar, N. A. Pertsev, and R. Waser, Phys. Rev. B **64**, 214103 (2001).
[50] B. S. Kwak, A. Erbil, J. D. Budai, M. F. Chisholm, L. A. Boatner, and B. J. Wilkens, Phys. Rev. B **49**, 14865 (1994).
[51] K. Lee and S. Baik, Annu. Rev. Mater. Res. **36**, 81 (2006).
[52] A. E. Romanov, W. Pompe, and J. S. Speck, J. Appl. Phys. **79**, 4037 (1996).
[53] N. A. Pertsev and A. G. Zembilgotov, J. Appl. Phys. **78**, 6170 (1995).
[54] N. A. Pertsev and A. G. Zembilgotov, J. Appl. Phys. **80**, 6401 (1996).
[55] S. P. Alpay and A. L. Roytburd, J. Appl. Phys. **83**, 4714 (1998).
[56] Z. G. Ban, S. P. Alpay, H. Feizhou, B. O. Wells, and X. X. Xi, Appl. Phys. Lett. **84**, 4848 (2004).
[57] B. S. Kwak, A. Erbil, B. J. Wilkens, J. D. Budai, M. F. Chisholm, and L. A. Boatner, Phys. Rev. Lett. **68**, 3733 (1992).
[58] C. M. Foster, Z. Li, M. Buckett, D. Miller, P. M. Baldo, L. E. Rehn, G. R. Bai, D. Guo, H. You, and K. L. Merkle, J. Appl. Phys. **78**, 2607 (1995).
[59] N. A. Pertsev and A. Y. Emelyanov, Appl. Phys. Lett. **71**, 3646 (1997).
[60] S. Y. Hu, Y. L. Li, and L. Q. Chen, J. Appl. Phys. **94**, 2542 (2003).
[61] D. Liu, M. Chelf, and K. W. White, Acta Mater. **54**, 4525 (2006).
[62] M.-W. Chu, I. Szafraniak, D. Hesse, M. Alexe, and U. Gosele, Phys. Rev. B **72**, 174112 (2005).
[63] I. B. Misirlioglu, A. L. Vasiliev, S. P. Alpay, M. Aindow, and R. Ramesh, J. Mater. Sci. **41**, 697 (2006).
[64] S. P. Alpay, A. S. Prakash, S. Aggarwal, P. Shuk, M. Greenblatt, R. Ramesh, and A. L. Roytburd, Scr. Mater. **39**, 1435 (1998).
[65] N. A. Pertsev and A. Y. Emel'yanov, Phys. Solid State **39**, 109 (1997).
[66] A. H. G. Vlooswijk, B. Noheda, G. Catalan, A. Janssens, B. Barcones, G. Rijnders, D. H. A. Blank, S. Venkatesan, B. Kooi, and J. T. M. de Hosson, Appl. Phys. Lett. **91**, 112901 (2007).
[67] M. Ahart, M. Somayazulu, R. E. Cohen, P. Ganesh, P. Dera, H. K. Mao, R. J. Hemley, Y. Ren, P. Liermann, and Z. G. Wu, Nature (London) **451**, 545 (2008).
[68] L. Q. Chen, in *Physics of Ferroelectrics: A Modern Perspective* (Springer, New York, 2007), Vol. 105, p. 363.
[69] K. Rabe, Ch. H. Ahn, and J.-M. Triscone, *Physics of Ferroelectrics* (Springer, New York, 2007).